Intelligent Automation & Soft Computing
DOI:10.32604/iasc.2021.01000
Article

SVSF-Based Robust UGV/UAV Control/Tracking Architecture in Disturbed Environment

Abdelatif Oussar[1,*], Abdelmoumen Ferrag[1], Mohamed Guiatni[1] and Mustapha Hamerlain[2]

[1]Ecole Militaire Polytechnique, Algiers, Algeria
[2]Centre de Développement des Technologies Avancées, Algiers, Algeria
[*]Corresponding Author: Abdelatif Oussar. Email: oussarabdelatif@gmail.com
Received: 04 December 2019; Accepted: 03 July 2020

Abstract: This paper presents the design of a robust architecture for the tracking of an unmanned ground vehicle (UGV) by an unmanned aerial vehicle (UAV). To enhance the robustness of the ground vehicle in the face of external disturbances and handle the non-linearities due to inputs saturation, an integral sliding mode controller was designed for the task of trajectory tracking. Stabilization of the aerial vehicle is achieved using an integral-backstepping solution. Estimation of the relative position between the two agents was solved using two approaches: the first solution (optimal) is based on a Kalman filter (KF) the second solution (robust) uses a smooth variable structure filter (SVSF). Simulations results, based on the full non-linear model of the two agents are presented in order to evaluate the performance and robustness of the proposed tracking architecture.

Keywords: UGV/UAV tracking; integral sliding mode controller; trajectory tracking; integral-backstepping controller; Kalman filter; robust smooth variable structure filter

Nomenclature

(x_r, y_r, θ_r):	Coordinates of UGV reference trajectory
(v_r, w_r):	UGV desired control inputs
(x, y, θ):	UGV actual coordinates
(v, w):	UGV control inputs
(δ_v, δ_w):	Uncertainties on v and w
r:	Radius of UGV wheels
$2L$:	The distance between the two driving wheels
$(\dot{\varphi}_d, \dot{\varphi}_l)$:	Angular velocity of the two driving wheels
(e_x, e_y, e_θ):	Tracking errors
(e_1, e_2, e_3):	Tracking errors expressed in the UGV frame
$\mathcal{U}_0, \mathcal{U}_1$:	Nominal and discontinuous part of the ISMC respectively
(v_{max}, w_{max}):	The bounds of the UGV controls
$s = [s_1, s_2]^T$:	Sliding surface
X_k:	State vector describing the UGV motion

T:	Sampling period
w_k:	Random process noise
z_k:	The measurements of the UGV position P_k
v_k:	Random measurement noise
$(x, y, z, \varphi, \theta, \psi)$:	Quadrotor position and orientation
(u_1, u_2, u_3, u_4):	Quadrotor control inputs
(u_x, u_y):	Quadrotor virtual control inputs

1 Introduction

Unmanned aerial/ground cooperation is increasingly attracting the attention of researchers. This is essentially due to the complementary skills provided by each type to overcome the specific limitations of each other. UGVs offer a higher payload and stronger calculation capabilities, while UAVs provide faster dynamics, and add a local coverage for the unseen areas from an aerial view [1]. Indeed, deployment of integrated multi-robot team consisting of heterogeneous robots provides advantages compared to strict homogeneous compositions. One of the attractive scenarios for multi-agent system is the tracking of a ground target using an unmanned aerial vehicle [2]. This allows performing important tasks like surveillance of convoys, reconnaissance, and intelligence missions [3]. Tracking ground targets is more difficult than aerial ones due to the topographic variations that can influence a target's motion patterns and obscurity to observation [4].

Many results related to this topic have been presented in the last few years. A circular pattern navigation algorithm for autonomous target tracking was presented in Rafi et al. [5] and Wise et al. [6], showing a good performance in simulation. Solutions based on partial information of the target state were presented in Peterson et al. [7], Summers et al. [8] and Kim et al. [9]. Observers, adaptive control, and extended Kalman filtering were used in this works for estimating the full target state. In Kim et al. [9] a non-linear model predictive controller was used to achieve the desired standoff configuration for an accelerating target. Quintero et al. [10] presented an output-feedback model predictive control with moving horizon estimation for target tracking by UAV, showing a good robustness.

Other works dealt with trajectory acquisition from video cameras, using particle filters for target estimation from non-stabilised cameras [11]. Multiple target tracking was achieved using Joint Probabilistic Data Association Filter (JPDAF) in the presence of unreliable target identification [12]. If a model for the object's motion is known, an observer can be used to estimate the object's velocity [13]. The recent work [14] covered one of the most important applications of estimation theory, namely, multi-target tracking, and included a thorough treatment of multisensor fusion and multiple hypothesis tracking, attribute-aided tracking, unresolved targets, sensor management, etc.

Air-ground collaborative systems find their applications in several fields. Authors in [15–21] present significant studies on Intelligence Surveillance and Reconnaissance (ISR) missions including both aerial and terrestrial vehicles. On the other hand, object tracking, path planning and localization are the others missions where this UAV/UGV cooperation is beneficial. We quote here some noteworthy studies [22–26] related with UAV/UGV systems collaborating to perform the above-mentioned tasks. As important part of this air-ground cooperation, many works have focused on "formation control" [27–29]. However, such hybrid UAV/UGV architecture can combine their tasks to achieve more complex missions [30–32].

More recently many studies have been made proposing new approaches to path planning for heterogeneous cooperating team (Air-ground Coordination). In Yulong et al. [33], Dubins path planning

combined with Traveling Salesman problem was proposed to find the shortest route. A Quaternion based control for circular UAV trajectory tracking, following a ground vehicle was proposed in Abaunza et al. [34].

Guastella et al. [35] designed a global path planning strategy for a UGV from aerial elevation maps for disaster response. Peterson et al. [36] the authors present a collaborative UAV/UGV system to online aerial terrain mapping to inform the ground vehicle's path planning in real time.

This kind of system can have practical applications for search and rescue missions. Some recent projects such as ICARUS [37] and ANKommEn [38] aims to develop a platform using multiple UAV and UGV for exploration of disaster scenarios for the detection of survivors and to provide maps in order to assist in maximizing the efficiency of Search and Rescue (SAR) operations.

In this paper, we first focus on the modeling and robust control of the two heterogeneous robots constituting the cooperative system. The second part covers the tracking problem of the ground agent by the UAV taking into account the dynamics of the aerial agent and the kinematics of the UGV. Since direct measurements are tainted with noise, it is essential to integrate an estimation filter allowing the prediction and estimation of the state of the ground target. We tested two estimation algorithms: the standard Kalman filter and the smooth variable structure filter.

The main contribution of this paper is the design of a new robust architecture for the tracking of an UGV by an UAV in order to deal with external disturbances and model uncertainties. To achieve this goal, the stabilization of the UAV is performed based on the integral-backstepping control approach while an integral sliding mode controller was designed for trajectory tracking. In addition, a comparative study of the proposed approaches for estimating the relative position between the two agents (UGV and UAV), is accomplished, illustrating the advantages of the proposed architecture.

The rest of this paper is organized as follows: in Section 2, the kinematic model of the UGV is presented and an integral sliding mode controller is designed in order to control the UGV motion. Section 3 provides the dynamic model of the UAV (quadrotor) together with the proposed control law based on the integral-backstepping approach. Section 4 presents the tracking algorithms used to estimate the state of the ground vehicle. In order to evaluate the proposed control and tracking architecture, simulation results with different scenarios are presented in Section 5.

2 UGV Modelling, Control and Trajectory Tracking

2.1 Formulation of the Trajectory Tracking Problem

We assume that the reference trajectory, generated by the motion planning algorithm, fulfils the following model:

$$\begin{bmatrix} \dot{x}_r \\ \dot{y}_r \\ \dot{\theta}_r \end{bmatrix} = \begin{bmatrix} \cos\theta_r & 0 \\ \sin\theta_r & 0 \\ 0 & 1 \end{bmatrix} \begin{bmatrix} v_r \\ w_r \end{bmatrix} \tag{1}$$

where x_r, y_r and θ_r represent the desired (x, y) position and orientation of the UGV, v_r and w_r are the desired linear and angular velocities respectively.

It is obvious that the real controls v and w rely on the state measurements x, y and θ (Fig. 1). Due to measurement noise and modeling uncertainties, here we consider input uncertainties for both v and w [39]. Thus, the real equation of the robot trajectory fulfills the following model:

$$\begin{bmatrix} \dot{x} \\ \dot{y} \\ \dot{\theta} \end{bmatrix} = \begin{bmatrix} \cos\theta & 0 \\ \sin\theta & 0 \\ 0 & 1 \end{bmatrix} \begin{bmatrix} v + \delta_v \\ w + \delta_w \end{bmatrix} \tag{2}$$

where the linear and angular velocities, v and w, are defined as follows:

$$v = \frac{r}{2}(\dot{\varphi}_d + \dot{\varphi}_l) \tag{3}$$

$$w = \frac{r}{2L}(\dot{\varphi}_d - \dot{\varphi}_l) \tag{4}$$

parameter r represents the radius of the wheels; $2L$ is the distance between the two driving wheels; $\dot{\varphi}_l$ and $\dot{\varphi}_d$ represent the angular velocity of two wheels left and right-hand side respectively; δ_v and δ_w are the uncertainties on v and w.

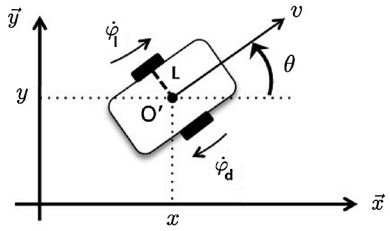

Figure 1: Unicycle-type mobile robot

The objective of trajectory tracking is to asymptotically stabilize the tracking errors $e_x = x_r - x$, $e_y = y_r - y$ and $e_\theta = \theta_r - \theta$ to zero.

Transforming the tracking errors expressed in the inertial frame to the robot frame, the error coordinates can be denoted as follows:

$$\begin{bmatrix} e_1 \\ e_2 \\ e_3 \end{bmatrix} = \begin{bmatrix} \cos\theta & \sin\theta & 0 \\ -\sin\theta & \cos\theta & 0 \\ 0 & 0 & 1 \end{bmatrix} \begin{bmatrix} e_x \\ e_y \\ e_\theta \end{bmatrix} \tag{5}$$

Thus, the tracking-error model is represented by the following equation:

$$\dot{e} = f_1(e) + f_2(e)(U + \delta) \tag{6}$$

where

$$\begin{cases} e = [e_1, e_2, e_3]^T \\ f_1(e) = [v_r \cos e_3, v_r \sin e_3, w_r]^T \\ f_2(e) = \begin{bmatrix} -1 & e_2 \\ 0 & -e1 \\ 0 & -1 \end{bmatrix} \\ U = [v, w]^T \text{ and } \delta = [\delta_v, \delta_w]^T \end{cases} \tag{7}$$

2.2 Integral Sliding Mode Controller Design

Sliding Mode Control (SMC) is widely used in the control of different type of systems, such as wheeled mobile robot [40], five DOF redundant robot [41], PH process in stirred tanks [42], tunnel bow thrusters [43]

or for other purpose such as multi-sensors data fusion [44]. In this part, we propose to enhance the SMC with the integral action, to improve its disturbances rejection. This controller is then applied to our UGV system.

For system Eq. (5), the control law is defined as follows:

$$\mathcal{U} = \mathcal{U}_0 + \mathcal{U}_1 \tag{8}$$

$\mathcal{U}_0$ is the nominal control and $\mathcal{U}_1$ represents the ISMC part which is designed to be discontinuous in order to reject the disturbance.

The first part of the control design is to find a saturated control law $\mathcal{U}_0$ so that the nominal system $\dot{e} = f_1(e) + f_2(e)\mathcal{U}_0$ is globally asymptotically stable (see Jiang et al. [45] for more details). The nominal control input is chosen as follows:

$$\mathcal{U}_0 = \begin{bmatrix} v_0 = v_r \cos e_3 + \lambda_3 \tanh e_1 \\ w_0 = w_r + \dfrac{\lambda_1 v_r e_2 \sin e_3}{e_3(1+e_1^2+e_2^2)} + \lambda_2 \tanh e_3 \end{bmatrix} \tag{9}$$

The positive parameters λ_1, λ_2 and λ_3 can be designed so that the bounds of the controls are complied with. This can be represented as follows:

$$|v_0| \leq v_{max} + \lambda_3, |w_0| \leq w_{max} + \frac{\lambda_1 v_{max}}{2} + \lambda_2 \tag{10}$$

For the ISMC part $\mathcal{U}_1$, the sliding variable 's' is defined as follows:

$$s = [s_1, s_2]^T = s_0(e) + z \tag{11}$$

where

$$\begin{cases} s_0(e) = [-e_1, -e_3]^T \\ \dot{z} = -\dfrac{\partial s_0}{\partial e}(f_1(e) + f_2(e)U_0) \\ z(0) = [e_1(0), e_3(0)]^T \end{cases} \tag{12}$$

The variable z includes the integral term and provides one more degree of freedom in the construction of the sliding variable. According to Defoort et al. [46], the sliding mode is established as the initial moment and the phase of convergence is eliminated. Then, the control law is given by the following equation:

$$U_1 = \begin{bmatrix} -K_1 sign(s_1) \\ -K_2 sign(-e_2 s_1 + s_2) \end{bmatrix} \tag{13}$$

with $K_1 > \delta_v + \mu$ and $K_2 > \delta_w + \mu$ such as: $\mu > 0$

In order to reduce the chattering phenomena, the *sign* function is replaced by: $f(x) = \dfrac{2}{\pi}\tanh(\eta x)$, with η being a positive constant [47]. Following from this, Eq. (13) can be written as follows:

$$U_1 = \begin{bmatrix} -\dfrac{2K_1}{\pi}\tanh(\eta_1 s_1) \\ -\dfrac{2K_2}{\pi}\tanh(\eta_2(-e_2 s_1 + s_2)) \end{bmatrix} \tag{14}$$

Remark 1: The trajectory evolves on the manifold $s = 0$ from $t = 0$ and remains there in presence of the disturbances. The time derivative of the sliding variable is $\dot{s} = \dfrac{\partial s_0}{\partial e}(\dot{e} - f_1(e) - f_2(e)\mathcal{U}_0)$. Therefore, the

motion equation in sliding mode is $\dot{e} = f_1(e) + f_2(e)\mathcal{U}_0$ which is globally asymptotically stable (see Defoort et al. [39] for more details).

2.3 Stability Analysis of the Smooth ISMC

Let us study the effect of the approximation of the *sign* function by *tanh* on global stability.

Lemma 1. [48] For every given scalar x and positive scalar η, the following inequality holds:

$$x\tanh(\eta x) = |x\tanh(\eta x)| = |x||\tanh(\eta x)| \geq 0$$

Proof of Lemma 1. According to the definition of *tanh* function, we have:

$$x\tanh(\eta x) = x\frac{e^{\eta x} - e^{-\eta x}}{e^{\eta x} + e^{-\eta x}} = \frac{1}{e^{2\eta x} + 1}x\left(e^{2\eta x} - 1\right)$$

Since

$$\begin{cases} e^{2\eta x} - 1 \geq 0 & \text{if} \quad x \geq 0 \\ e^{2\eta x} - < 0 & \text{if} \quad x < 0 \end{cases} \quad \text{Then} \quad x\left(e^{2\eta x} - 1\right) \geq 0$$

Therefore

$$x\tanh(\eta x) = \frac{1}{e^{2\eta x} + 1}x\left(e^{2\eta x} - 1\right) \geq 0$$

And

$$x\tanh(\eta x) = |x\tanh(\eta x)| = |x||\tanh(\eta x)| \geq 0$$

Proof of stability. Consider the following Lyapunov function candidate:

$$V = \tfrac{1}{2}s^T s$$

The discontinuous control term must satisfy the condition $\dot{V} \leq 0$ guaranteeing the global asymptotic stability.

$$\dot{V} = s^T\dot{s} = s^T(\dot{s}_0(e) + \dot{z})$$

$$\dot{V} = s^T\left[\frac{\partial s_0}{\partial e}\dot{e} - \frac{\partial s_0}{\partial e}(f_1(e) + f_2(e))U_0\right]$$

$$\dot{V} = s^T\frac{\partial s_0}{\partial e}f_2(e)(U_1 + \delta)$$

$$\dot{V} = (\, s_1 \quad -e_2 s_1 + s_2\,)(U_1 + \delta)$$

According to Lemma 1, the above condition is satisfied if:

$$U_1 = \begin{bmatrix} -\dfrac{2K_1}{\pi}\tanh(\eta_1 s_1) \\ -\dfrac{2K_2}{\pi}\tanh(\eta_2(-e_2 s_1 + s_2)) \end{bmatrix}$$

with $\dfrac{2K_1}{\pi} > \delta_v + \mu$ and $\dfrac{2K_2}{\pi} > \delta_w + \mu$ $(\mu > 0\,)$

Therefore, according to LaSalle's theorem, the control system with the smoothed ISMC is asymptotically stable in the sense of Lyapunov.

2.4 Tracking Algorithm based on Kalman Filter

Ground targets (UGVs) were always implicitly assumed to be non-manoeuvring and the noise statistics involved in the dynamics model/target observation (matrices $Q(k)$ and $R(k)$) were assumed to be known. In practice, it goes without saying that these parameters are never well known and may vary over time depending on the manoeuvring capacity of the ground targets. For this reason, we have opted for the use of a discrete kinematic model with quasi-constant acceleration [49]. We can model the equations of the UGV as a linear system in following representation:

$$X_{k+1} = AX_k + \Gamma w_k \tag{15}$$

where:

$$A = \begin{bmatrix} 1 & T & \frac{1}{2}T^2 & 0 & 0 & 0 \\ 0 & 1 & T & 0 & 0 & 0 \\ 0 & 0 & 1 & 0 & 0 & 0 \\ 0 & 0 & 0 & 1 & T & \frac{1}{2}T^2 \\ 0 & 0 & 0 & 0 & 1 & T \\ 0 & 0 & 0 & 0 & 0 & 1 \end{bmatrix} \tag{16}$$

$$\Gamma = \begin{bmatrix} \frac{1}{2}T^2 & 0 \\ T & 0 \\ 1 & 0 \\ 0 & \frac{1}{2}T^2 \\ 0 & T \\ 0 & 1 \end{bmatrix} \tag{17}$$

and w_k is the random process noise. X_k is the state vector describing the motion of the UGV (its position, velocity and acceleration):

$$X_k = [\, x_k \quad \dot{x}_k \quad \ddot{x}_k \quad y_k \quad \dot{y}_k \quad \ddot{y}_k \,]^T$$

and T is the sampling period. The measurements of the mobile robot position p at time k are described as follows:

$$Z_k = H_k p_k + v_k \tag{18}$$

where v_k is a random measurement noise. We assume that the process and measurement noises w_k and v_k are white, zero-mean.

As the measurement vector is the UGV position (x_k, y_k), the matrix H_k in Eq. (18) (called measurement matrix) is given by:

$$H_k = \begin{pmatrix} 1 & 0 & 0 & 0 & 0 & 0 \\ 0 & 0 & 0 & 1 & 0 & 0 \end{pmatrix}$$

The predicting and update equations for the Kalman filter are presented as follows:

$$\begin{cases} \hat{X}_{k+1|k} = A_k \hat{X}_{k|k} \\ P_{k+1|k} = A_k P_{k|k} A_k^T + Q_k \\ \tilde{y}_{k+1} = Z_k - H_k X_{k+1|k} \\ S_{k+1} = H_{k+1} P_{k+1|k} H_{k+1}^T + R_{k+1} \\ K_{k+1} = P_{k+1|k} H_{k+1}^T S_{k+1}^{-1} \\ \hat{X}_{k+1|k+1} = \hat{X}_{k+1|k} + K_k \tilde{y}_{k+1} \\ P_{k+1|k+1} = (I - K_{k+1} H_{k+1}) P_{k+1|k} \end{cases} \tag{19}$$

Let us describe the Kalman filter parameters (X_0, R_k, Q_k and P_0) selection:

- For the initialization (X_0,P_0), several simulations were performed by considering initialization accuracy up to 70% the true value of the UGV position. We have noticed that the results of the estimation and the convergence speed of the filter are highly dependent on initialization. The suitable values of (X_0,P_0) are estimated after many simulations.
- The selection of matrices R_k and Q_k requires prior knowledge of measurement and process noises. The covariance of measurement noise v_k can be expressed as:

$R_k = \begin{pmatrix} \sigma_x^2 & 0 \\ 0 & \sigma_y^2 \end{pmatrix}$; where σ_x and σ_y are the standard deviations of the position of x and y, respectively. In our case, the sensor used to measure the UGV position is assumed to be a camera embedded on the UAV. Thus, in our simulations the matrix R_k is selected based on real camera characteristics.

The covariance matrix of the process noise (Q_k) is estimated based on the odometer model of the mobile robot given by Eq. (2), in our simulation a suitable values of the matrix Q_k are determined from a real robot (Pioneer 3-AT).

3 Quadrotor Dynamics and Control

3.1 Quadrotor Modeling

Our interest in such type of UAV (Fig. 2) is its hovering capability and high manoeuverability.

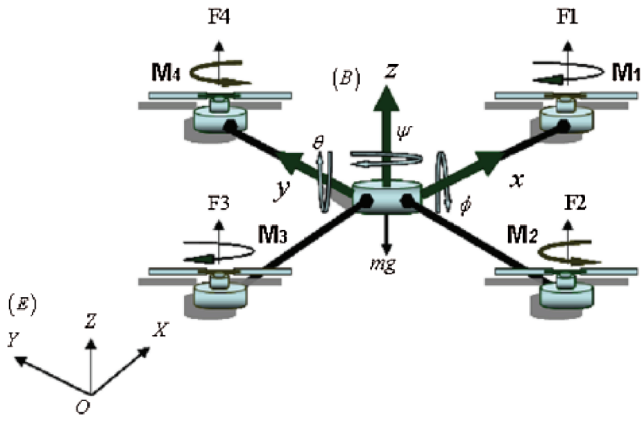

Figure 2: Quadrotor configuration

The dynamic models of the quadrotor are well studied. The details of the following Newton-Euler equations can be found in Refs. [50–53].

$$\begin{cases} \ddot{\phi} = \dfrac{J_y - J_z}{J_x}\dot{\theta}\dot{\psi} - \dfrac{J_r}{J_x}\bar{\Omega}\dot{\theta} - \dfrac{K_{fax}}{J_x}\dot{\phi}^2 + \dfrac{1}{J_x}u_2 \\ \ddot{\theta} = \dfrac{J_z - J_x}{J_y}\dot{\phi}\dot{\psi} + \dfrac{J_r}{J_y}\bar{\Omega}\dot{\phi} - \dfrac{K_{fay}}{J_y}\dot{\theta}^2 + \dfrac{1}{J_y}u_3 \\ \ddot{\psi} = \dfrac{J_x - J_y}{J_z}\dot{\theta}\dot{\phi} - \dfrac{K_{faz}}{J_z}\dot{\psi}^2 + \dfrac{1}{J_z}u_4 \\ \ddot{x} = \dfrac{-K_{ftx}}{m}\dot{x} + \dfrac{1}{m}u_x u_1 \\ \ddot{y} = \dfrac{-K_{fty}}{m}\dot{y} + \dfrac{1}{m}u_y u_1 \\ \ddot{z} = \dfrac{-K_{ftz}}{m}\dot{z} - g + \dfrac{1}{m}(\cos\phi\cos\theta)u_1 \end{cases} \tag{20}$$

The control inputs of the UAV are defined as follows:

$$\begin{cases} u_1 = b(w_1^2 + w_2^2 + w_3^2 + w_4^2) \\ u_2 = lb(w_4^2 - w_2^2) \\ u_3 = lb(w_3^2 - w_1^2) \\ u_4 = d(w_1^2 - w_2^2 + w_3^2 - w_4^2) \\ u_x = (\cos\phi\cos\psi\sin\theta + \sin\phi\sin\psi) \\ u_y = (\cos\phi\sin\psi\sin\theta - \sin\phi\cos\psi) \\ \bar{\Omega} = (w_1 - w_2 + w_3 - w_4) \end{cases} \tag{21}$$

The description of the parameters used in this model is given in Tab. 1.

Table 1: Quadrotor parameters description

Symbol	Description
m	Mass of quadrotor
g	Gravity
l	distance between the centre of mass and the rotation axis of the engines
J_x	Inertia moment along x axis
J_y	Inertia moment along y axis
J_z	Inertia moment along z axis
K_{fa}	Coefficients of aerodynamics frictions
K_{ft}	Drag force coefficients according to (x, y, z) axis
b	Lift force coefficient
d	Drag force coefficient
J_r	Rotor inertia

3.2 Backstepping Controller (BC) Design

In order to control the UAV a backstepping control scheme is used. The inner controller stabilizes the orientation angles in order to achieve a stable flight while the outer controller is responsible for the control of the position of UAV. Further the state vector of the UAV is defined as follows:

$$X = [\phi, \dot{\phi}, \theta, \dot{\theta}, \psi, \dot{\psi}, z, \dot{z}, x, \dot{x}, y, \dot{y}]^T = [x_1, x_2, x_3, x_4, x_5, x_6, x_7, x_8, x_9, x_{10}, x_{11}, x_{12}]^T$$

Thus we obtain the following equations:

$$\begin{cases} \dot{x}_1 = x_2 \\ \dot{x}_2 = a_1 x_4 x_6 + a_2 x_2^2 + a_3 \bar{\Omega} x_4 + b_1 u_2 \\ \dot{x}_3 = x_4 \\ \dot{x}_4 = a_4 x_2 x_6 + a_5 x_4^2 + a_6 \bar{\Omega} x_2 + b_2 u_3 \\ \dot{x}_5 = x_6 \\ \dot{x}_6 = a_7 x_2 x_4 + a_8 x_6^2 + b_3 u_4 \\ \dot{x}_7 = x_8 \\ \dot{x}_8 = a_9 x_8 - g + \dfrac{1}{m}(\cos x_1 \cos x_3) u_1 \\ \dot{x}_9 = x_{10} \\ \dot{x}_{10} = a_{10} x_{10} + \dfrac{1}{m} u_x u_1 \\ \dot{x}_{11} = x_{12} \\ \dot{x}_{12} = a_{11} x_{12} + \dfrac{1}{m} u_y u_1 \end{cases} \tag{22}$$

with

$$\begin{cases} a_1 = \dfrac{J_y - J_z}{J_x}, a_2 = -\dfrac{K_{fax}}{J_x}, a_3 = -\dfrac{J_r}{J_x}, a_4 = \dfrac{J_z - J_x}{J_y}; \\ a_5 = -\dfrac{K_{fay}}{J_y}, a_6 = \dfrac{J_r}{J_y}, a_7 = -\dfrac{J_x - J_y}{J_z}, a_8 = -\dfrac{K_{faz}}{J_z}; \\ a_9 = -\dfrac{K_{ftz}}{m}, a_{10} = -\dfrac{K_{ftx}}{m}, a_{11} = -\dfrac{K_{fty}}{m}; \\ b_1 = \dfrac{1}{J_x}, b_2 = \dfrac{1}{J_y}, b_3 = \dfrac{1}{J_z} \end{cases}$$

The following Lyapunov functions are used:

$$V_i = \begin{cases} \frac{1}{2} z_i^2 & /i \in \{1,3,5,7,9,11\} \\ \frac{1}{2}(V_{i-1} + z_i^2) & /i \in \{2,4,6,8,10,12\} \end{cases} \tag{23}$$

with

$$z_i = \begin{cases} x_{id} - x_i & /i \in \{1,3,5,7,9,11\} \\ x_i - \dot{x}_{(i-1)d} - \alpha_{(i-1)} z_{(i-1)} & /i \in \{2,4,6,8,10,12\} \end{cases}$$

The application of the backstepping technique [50] and [54] on the quadrotor state model give the following control inputs:

$$\begin{cases} u_1 = \dfrac{m}{\cos x_1 \cos x_3}\begin{pmatrix} z_7 - a_9 x_8 + g \\ -\alpha_7(z_8 + \alpha_7 z_7) - \alpha_8 z_8 + \ddot{x}_{7d} \end{pmatrix} \\ u_2 = \dfrac{1}{b_1}\begin{pmatrix} z_1 - a_1 x_4 x_6 - a_2 x_2^2 - a_3 \bar{\Omega} x_4 \\ -\alpha_1(z_2 + \alpha_1 z_1) - \alpha_2 z_2 + \ddot{x}_{1d} \end{pmatrix} \\ u_3 = \dfrac{1}{b_2}\begin{pmatrix} z_3 - a_4 x_2 x_6 - a_5 x_4^2 - a_6 \bar{\Omega} x_2 \\ -\alpha_3(z_4 + \alpha_3 z_3) - \alpha_4 z_4 + \ddot{x}_{3d} \end{pmatrix} \\ u_4 = \dfrac{1}{b_3}\begin{pmatrix} z_5 - a_7 x_2 x_4 - a_8 x_6^2 \\ -\alpha_5(z_6 + \alpha_5 z_5) - \alpha_6 z_6 + \ddot{x}_{5d} \end{pmatrix} \\ u_x = \dfrac{m}{u_1}\begin{pmatrix} z_9 - a_{10} x_{10} - \alpha_9(z_{10} + \alpha_9 z_9) \\ -\alpha_{10} z_{10} + \ddot{x}_{9d} \end{pmatrix} \\ u_y = \dfrac{m}{u_1}\begin{pmatrix} z_{11} - a_{11} x_{12} - \alpha_{11}(z_{12} + \alpha_{11} z_{11}) \\ -\alpha_{12} z_{12} + \ddot{x}_{11d} \end{pmatrix} \end{cases} \tag{24}$$

with $\cos x_1 \cos x_3 \neq 0, \alpha_i > 0$ and $\forall i \in \{1, 2\ldots, 12\}$. Variables u_x and u_y are virtual control inputs which will be used to find desired Euler angles as follows:

$$\begin{cases} \phi_d = x_{1d} = \arcsin(u_x \sin x_{5d} - u_y \cos x_{5d}) \\ \theta_d = x_{3d} = \arcsin\left(\dfrac{u_x \cos x_{5d} + u_y \sin x_{5d}}{\cos x_{1d}}\right) \end{cases} \tag{25}$$

3.3 Simulation Results (I)

The simulation results are obtained based on the following realistic parameters of quadrotor in Tab. 2 and characteristics of Pioneer 3-AT mobile robot in Tab. 3.

Table 2: Quadrotor general parameters [50]

Symbol	Values and unit
m	0.65 kg
l	0.23 m
J_x	$7,5.10^{-3}$ kg.m^2
J_y	$7,5.10^{-3}$ kg.m^2
J_z	$1,3.10^{-2}$ kg.m^2
K_{fa}	$diag[5,567 \quad 5,567 \quad 6,354] \cdot 10^{-4}$ N/rad/s
K_{ft}	$diag[0.032 \quad 0.032 \quad 0.048]$ N/m/s
b	$3,13.10^{-5}$ N/rad/s
d	$7,5.10^{-7}$ N.m/rad/s
J_r	6.10^{-5} kg.m^2

In this first simulations set, we aim to evaluate the ISMC controller of the ground agent (UGV), thus the first tracking approach based on the Kalman filter and the backstepping control of the quadrotor.

In this context of the ground agent tracking by a UAV, and in order to get closer to reality, several scenarios are considered as follows.

- The initial conditions of the UGV: $x_0 = 0.5 \quad y_0 = -0.5 \quad \theta_0 = \dfrac{\pi}{4}$

- The initial conditions of the quadrotor: $x_0 = -0.5 \quad y_0 = -0.5 \quad z_0 = 0$
- The control inputs of the quadrotor are bounded as follows:

$$\begin{cases} 0 \le u_1 \le 4b\Omega_{max}^2 \\ |u_2| \le lb\Omega_{max}^2 \\ |u_3| \le lb\Omega_{max}^2 \\ |u_4| \le 2d\Omega_{max}^2 \end{cases} \tag{26}$$

Table 3: Characteristics of the Pioneer 3-AT

Feature	Description
Dimensions	508 mm long, 497 mm large, 277 mm high
Weight	12 kg, operating payload of 12 kg on floor
Batteries	2–4 hours, up to 3 lead acid batteries of 7.2 Ah each, 12 V
Skid steering drive	Turn radius (0 cm), swing radius (34 cm)
Speed	Max, forward/backward speed (0.8 m/s), rotation speed (140 deg/s)

- The initial parameters of the Kalman estimator are given as follows:

$$\begin{cases} X_0 = [0.4 \quad 0 \quad 0 \quad -0.4 \quad 0 \quad 0] \\ R_k = diag\left(\left[0.05^2 \quad 0.03^2\right]\right) \\ Q_k = \Gamma\left(5.10^{-3}\right)^2\Gamma^T \\ P_0 = zeros(6,6) \end{cases} \tag{27}$$

Scenario 1: The quadrotor may be affected by external disturbances such as wind. Several models of wind are proposed in Gawronski [55]. In our work, we assume that the wind has caused the same acceleration intensity on all axes x, y and z [56], as shown in Fig. 3. The mathematical model of wind is given by the following equation:

$$a(t) = \begin{cases} 0 & \text{when} \quad 0s < t \le 30s \\ 0.7\sin(\frac{\pi(t-30)}{31}) + 0.4\sin(\frac{\pi(t-30)}{7}) \cdots & \\ \cdots + 0.08\sin(\frac{\pi(t-30)}{2}) + 0.056\sin(\frac{24\pi(t-30)}{11}) & \text{when} \quad 30s < t \le 41s \\ 0 & \text{when} \quad 41s < t \le 45s \\ 3.35\sin(\frac{\pi(t-45)}{21}) + 0.5\sin(\frac{\pi(t-45)}{2}) \cdots & \\ \cdots + 0.45\sin(\frac{\pi(t-45)}{5}) + 0.205\sin(\frac{24\pi(t-45)}{11}) & \text{when} \quad 45s < t \le 65s \\ 0 & \text{when} \quad 60s < t \le 70s \end{cases} \tag{28}$$

- **Scenario 2**: This scenario is designed to evaluate the robustness of the control system with respect to modelling errors and measurement noises. In terms of parametric uncertainty, we assume that the elements of the inertia matrix J_x , J_y and J_z are underestimated to 60%, the coefficients b and d are also underestimated, whereas the values used in the control are only 80% of the actual values.

$$\begin{cases} \tilde{J}_x = 0.6J_x \\ \tilde{J}_y = 0.6J_y \\ \tilde{J}_z = 0.6J_z \\ \tilde{b} = 0.8b \\ \tilde{d} = 0.8d \end{cases} \tag{29}$$

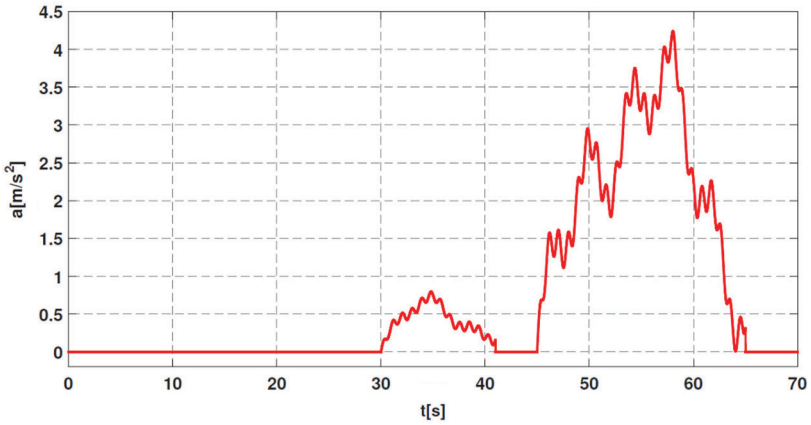

Figure 3: Time evolution of wind acceleration

As for the measurement noises, an additive Gaussian white noise with the density 150 μg/Hz was considered.

In the presence of wind gusts (Fig. 3) and as shown in Fig. 4, the quadrotor tracks the UGV that traveled Eight trajectory using the ISMC controller. By looking at Figs. 5 and 6, it can be noticed that the ISMC allows the robot to follow the set point correctly according to the two axes x, y and accounts for the saturation constraints with a very low tracking error on the trajectory realized by the UGV. The two sliding surfaces (s_1, s_2) tend to zero at the initial moment. Figs. 7 and 8 show that the wind affects the performances of the quadrotor during its mission, resulting in maximum absolute tracking errors of 0.27 m along z, 0.18 m along x and y.

As for scenario 1, even with the existence of parametric uncertainties and measurement noises, the quadrotor succeeds in tracking the mobile robot with small fluctuations in its tracking trajectory (Fig. 9). The tracking error along x axis takes a value of approximately 0.35 m, which shows that these disturbances have significant effects on the control by backstepping as indicated in Figs. 10 and 11.

4 Robust Control/Tracking Architecture

4.1 Robust Tracking algorithm based on SVSF

One of the major challenges for the tracking algorithm is the uncertainty in the motion of UGV. This uncertainty refers to the fact that a precise dynamic model of the movement is not available at the level of the tracking algorithm [57,58]. However, the Kalman filter (KF) can only achieve a good performance (optimal solution) under the assumption that the complete and exact information of the process model and the noise distribution are to be known as a prior. In practice, state and observation models are often poorly known, or contain uncertain parameters, and the statistical properties of noise (state and observation) are also poorly known, coming to the optimality of the solution obtained. Therefore, to improve our tracking algorithm, and to overcome these limitations, we propose to use a new filter or estimator called Smooth Variable Structure Filter (SVSF) to process the tracking problem of a UGV [59,60].

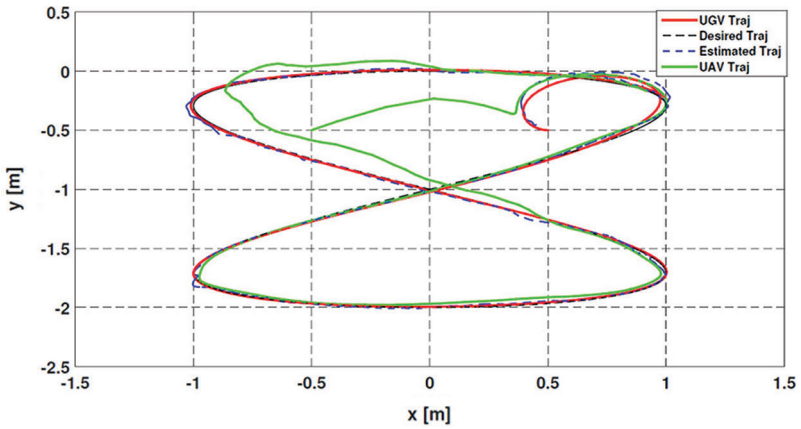

(a)

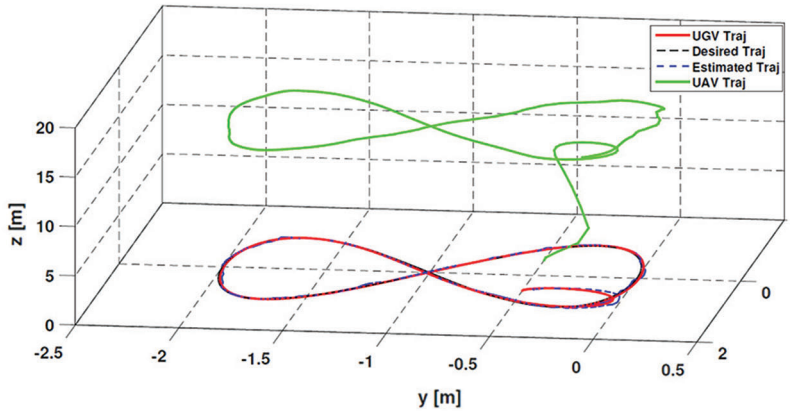

(b)

Figure 4: Tracking of UGV by the quadrotor in the presence of wind: (a) 2D, (b) 3D

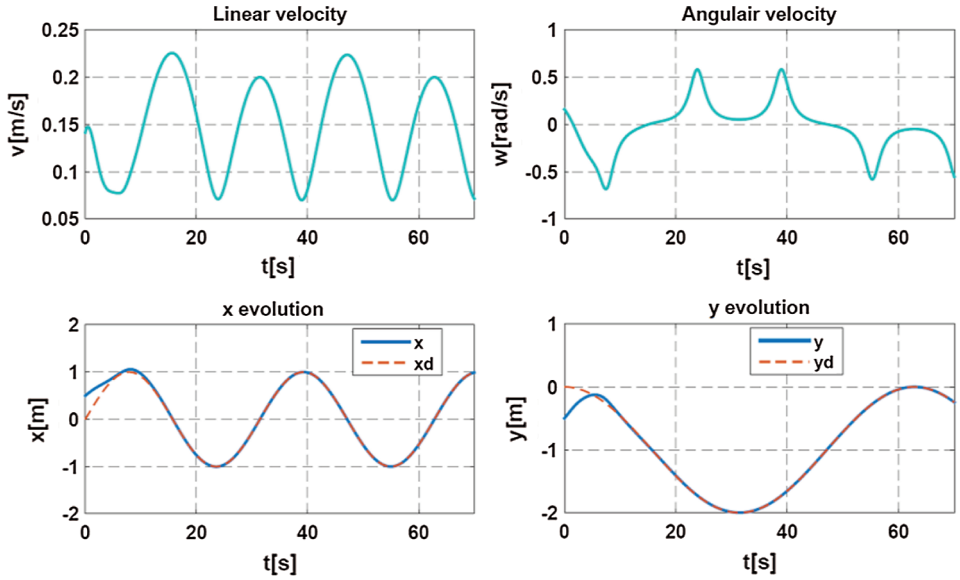

Figure 5: Evolution in time of the mobile robot position and control inputs

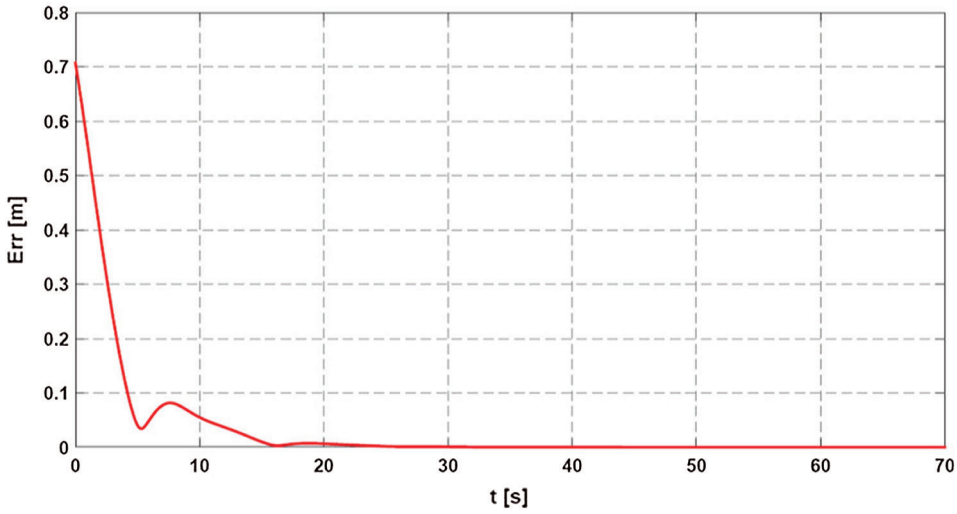

(a)

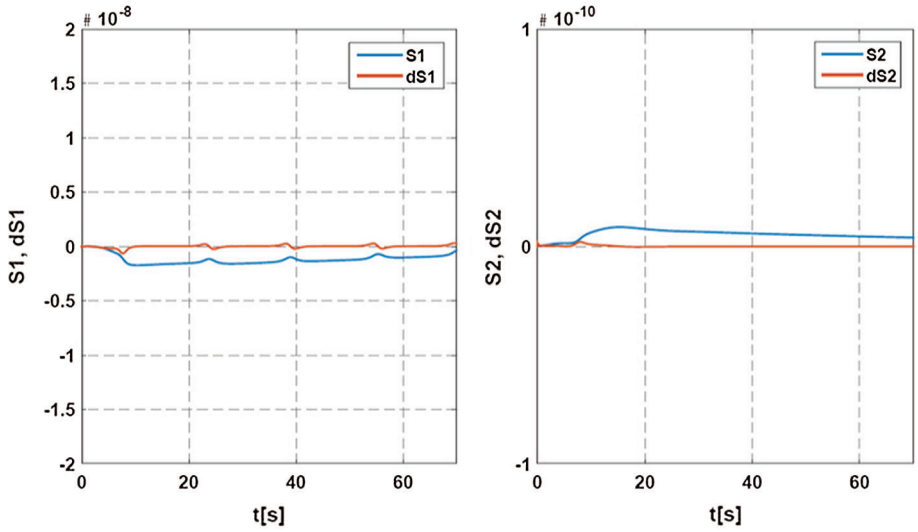

(b)

Figure 6: Evolution in time of: (a) Tracking error (b) The sliding surfaces

The Smooth Variable Structure Filter is a relatively new estimating strategy proposed by Habibi in 2007 [61]. This strategy is based on the concepts of sliding mode control and the theory of systems with variable structure, outcome and similar design to variable structure filter (VSF) [62]. This filter is formulated in the predictive-correction format, and can be used for linear or non-linear systems. It uses a correction gain simpler than the one used by the VSF. The SVSF is introduced to provide more stability and robustness to the estimation process. This technique is generally used for the estimation of states and parameters of dynamic systems [63], the prediction and diagnosis of defects in systems [64] and targets tracking problems [59,60,65].

To formulate the tracking problem, we use the same model that has been described in detail by the two Eqs. (15) and (18).

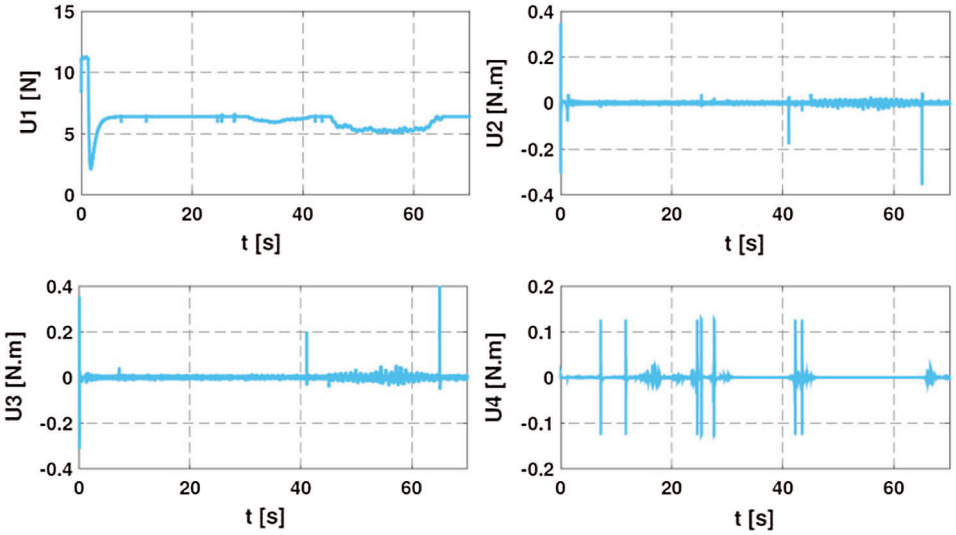

Figure 7: Control inputs of the quadrotor in the presence of wind disturbance (scenario 1)

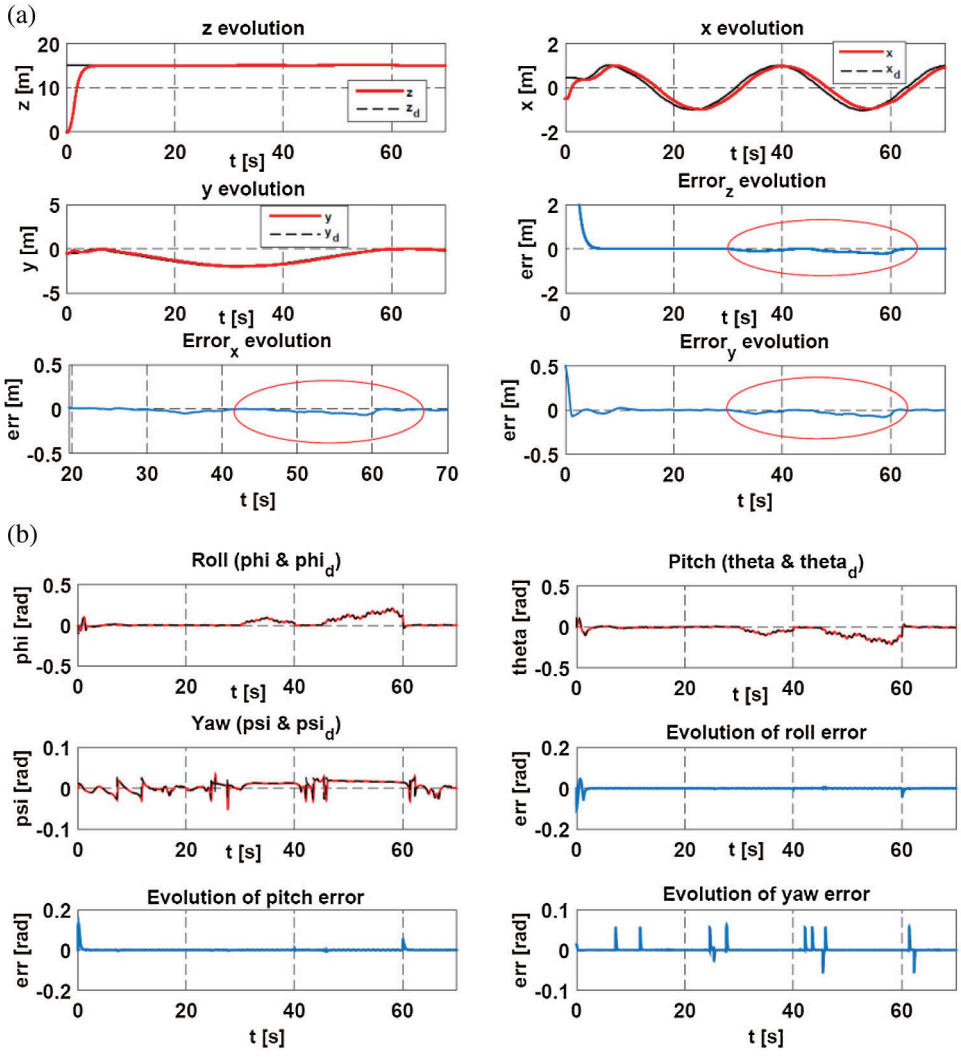

Figure 8: Evolution of the quadrotor: (a) Translation (x,y,z) (b) Orientation angles (scenario 1)

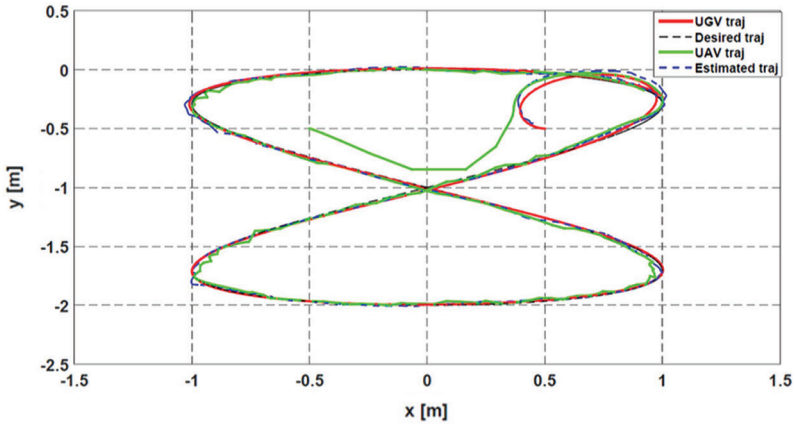

(a)

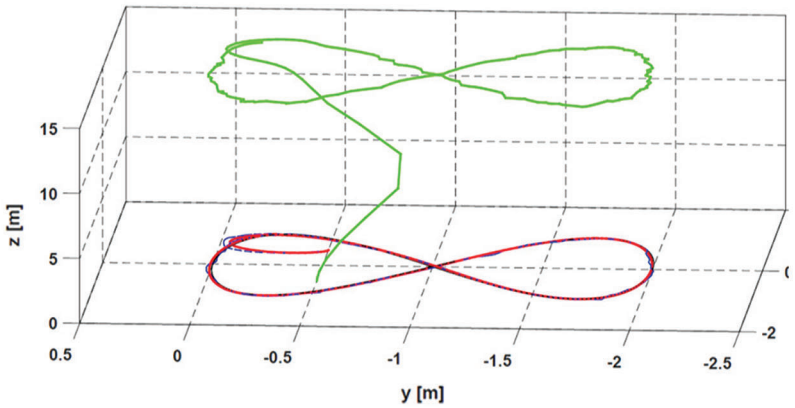

(b)

Figure 9: Tracking of UGV by the quadrotor with parametric uncertainties and measurement noise: (a) 2D, (b) 3D

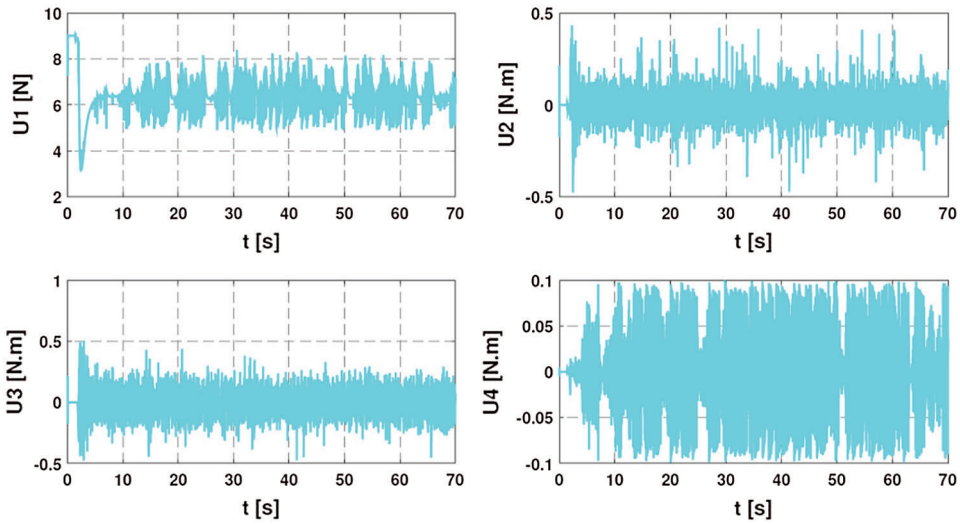

Figure 10: The control inputs of the quadrotor (scenario 2)

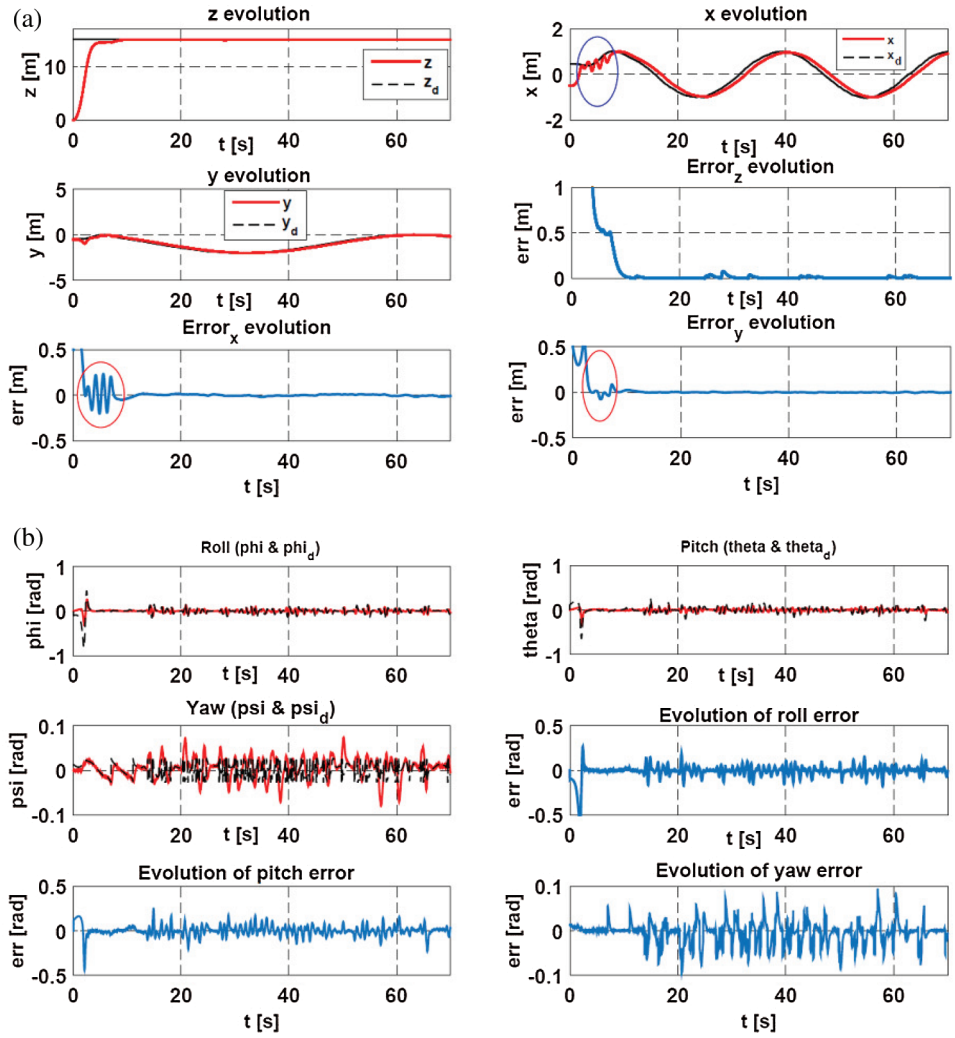

Figure 11: Evolution of the quadrotor: (a) Translation (x,y,z) (b) Orientation angles (scenario 2)

The SVSF estimation method is described by the following series of equations. Note that this formulation includes state error covariance equations as presented in Gadsden et al. [66], which was not originally presented in the standard SVSF form [61]. The prediction stage is similar to the KF; its steps are as follows:

- Initialization

$$\begin{cases} \hat{X}_{0|0} = X_0 \\ \hat{E}_{0|0} = E_0 \end{cases} \tag{30}$$

- Prediction

$$\hat{X}_{k+1|k} = A_k \hat{X}_{k|k} \tag{31}$$

$$P_{k+1|k} = A_k P_{k|k} A_k^T + Q_k \tag{32}$$

where $\hat{X}_{k|k}$ is the state estimated at time k of the state $X_{k|k}$.

$$\hat{Y}_{k+1|k} = H\hat{X}_{k+1|k} \tag{33}$$

then, pretest measurement error is calculated by the following equation:

$$E_{k+1|k} = Y_{k+1} - \hat{Y}_{k+1|k} \tag{34}$$

- Update

For the state estimate, the SVSF correction gain is calculated by MacArthur et al. [22] and Phan et al. [31]:

$$K_{k+1|k} = H^{+}Diag[(|E_{k+1|k}|_{abs} + \gamma|E_{k|k}|_{abs})^{\circ}Sat(\bar{\Psi}^{-1}E_{k+1|k})][Diag(E_{k+1|k})]^{-1} \tag{35}$$

where $^{\circ}$ signifies *Schur* (or element-by-element) multiplication, the superscript + refers to the pseudo inverse of a matrix and $\bar{\Psi}^{-1}$ is a diagonal matrix constructed from the smoothing boundary layer vector Ψ, defined as follows:

$$\bar{\Psi}^{-1} = [Diag(\Psi)]^{-1} = \begin{bmatrix} \frac{1}{\Psi_1} & 0 & 0 \\ 0 & \ddots & 0 \\ 0 & 0 & \frac{1}{\Psi_m} \end{bmatrix} \tag{36}$$

The form of saturation used in Eq. (35) is defined as follows:

$$Sat(\bar{\Psi}^{-1}E_{k+1|k}) = \begin{cases} \frac{E^i_{k+1|k}}{\Psi_i} \geq 1 \\ -1 < \frac{E^i_{k+1|k}}{\Psi_i} < 1 \\ \frac{E^i_{k+1|k}}{\Psi_i} \leq -1 \end{cases} \tag{37}$$

The gain is used to update the predicted state as follows:

$$\hat{X}_{k+1|k+1} = \hat{X}_{k+1|k} + K_{k+1|k}E_{k+1|k} \tag{38}$$

The covariance associated with the state updates is then calculated as follows:

$$P_{k+1|k+1} = [I - K_{k+1|k}H_K]P_{k+1|k}[I - K_{k+1|k}H_K]^T + K_{k+1|k}R_{k+1}K^T_{k+1|k} \tag{39}$$

Thus, the estimated measurement and the corresponding empirical measurement error are calculated as follows:

$$\begin{cases} \hat{Y}_{k+1|k+1} = H\hat{X}_{k+1|k+1} \\ E_{k+1|k+1} = Y_{k+1} - \hat{Y}_{k+1|k+1} \end{cases} \tag{40}$$

Two critical variables in this process are the pretest and empirical measurements (output) error estimates, defined by Eqs. (34) and (40). It shall be noted that Eq. (40) is the empirical measurement error estimates from the previous time step, and is used only in the gain calculation.

The selection of the smoothing boundary layer width vector Ψ reflects the level of uncertainties in the filter and the disturbances (i.e., system and measurement noise, and uncertain parameters).

4.2 Integral-Backstepping Controller (IBC)

The backstepping control cannot ensure the favorable tracking performance of the quadrotor if unpredictable disturbances from the unknown external disturbance, modeling errors, as well as measurement noise occur. In order to improve these performances and consequently the robustness, we propose to combine the conventional PID with the backstepping control. This will allow for integral backstepping. However, this control technique has been proposed in several research studies [50,52,67,68,69], which demonstrated that the integral backstepping controller allows rejection of external disturbances and is robust to parametric uncertainties.

The application of the integral backstepping control on the quadrotor state model gives the following control inputs:

$$\begin{cases} u_1 = \dfrac{m}{\cos x_1 \cos x_3}\left(z_7 - a_9 x_8 + g + \ddot{x}_{7d} - \alpha_7(\alpha_7 z_7 + z_8 + \lambda_4 \chi_4) + \lambda_4 z_7 - \alpha_8 z_8\right) \\ u_2 = \dfrac{1}{b_1}\left(z_1 - a_1 x_4 x_6 - a_2 x_2^2 - a_3 \bar{\Omega} x_4 + \ddot{x}_{1d} - \alpha_1(\alpha_1 z_1 + z_2 + \lambda_1 \chi_1) + \lambda_1 z_1 - \alpha_2 z_2\right) \\ u_3 = \dfrac{1}{b_2}\left(z_3 - a_4 x_2 x_6 - a_5 x_4^2 - a_6 \bar{\Omega} x_2 + \ddot{x}_{3d} - \alpha_3(\alpha_3 z_3 + z_4 + \lambda_2 \chi_2) + \lambda_2 z_3 - \alpha_4 z_4\right) \\ u_4 = \dfrac{1}{b_3}\left(z_5 - a_7 x_2 x_4 - a_8 x_6^2 + \ddot{x}_{5d} - \alpha_5(\alpha_5 z_5 + z_6 + \lambda_3 \chi_3) + \lambda_3 z_5 - \alpha_6 z_6\right) \\ u_x = \dfrac{m}{u_1}\left(z_9 - a_{10} x_{10} - \alpha_9(z_{10} + \alpha_9 z_9 + \lambda_5 \chi_5) + \lambda_5 z_9 - \alpha_{10} z_{10} + \ddot{x}_{9d}\right) \\ u_y = \dfrac{m}{u_1}\left(z_{11} - a_{11} x_{12} - \alpha_{11}(z_{12} + \alpha_{11} z_{11} + \lambda_6 \chi_6) + \lambda_6 z_1 1 - \alpha_{12} z_{12} + \ddot{x}_{11d}\right) \end{cases} \tag{41}$$

Such as:

$$\begin{cases} \alpha_i > 0 & \forall i \in \{1,2,3 \ldots 12\} \\ z_j = x_{jd} - x_j & /j \in \{1,3,5,7,9,11\} \\ \dot{\chi}_j = z_j \end{cases} \tag{42}$$

and the Lyapunov functions take the following form:

$$V_i = \begin{cases} \dfrac{1}{2} z_i^2 + \dfrac{\lambda_j}{2} \chi_i^2 & /i \in \{1,3,5,7,9,11\} \\ & j \in \{1,2,3 \ldots 6\} \\ V_{i-1} + \dfrac{1}{2} z_i^2 & /i \in \{2,4,6,8,10,12\} \end{cases} \tag{43}$$

For the selection of the controller parameters, we have used an approach based on PSO (Particle Swarm Optimization) optimization method, more details can be found in Yacef et al. [70].

5 Simulation Results (II)

5.1 Comparative Study KF/SVSF

After explaining and presenting the various tracking algorithms (KF and SVSF), showing the principle and the mathematical development. Their estimation accuracy and robustness to different types of noise will be evaluated. The root mean square error (RMSE) of the different results is calculated for different scenarios.

Scenario 3: In this scenario, the favorable conditions for the Kalman filter will be placed, by applying on the states and on the obtained measurements decorrelated centered noises as covariance matrix:

$$\begin{cases} Q_k = \Gamma(2.10^{-2})^2\Gamma^T \\ R_k = Diag([0.05^2; 0.05^2]) \end{cases} \tag{44}$$

The γ, Ψ matrices used and the initial states X_0, P_0 are as follows:

$$\begin{cases} \gamma = Diag([0.8; 0.8]) \\ \Psi = Diag([6; 5]) \\ X_0 = [0.4; 0; 0; -0.4; 0; 0] \\ P_0 = 10 \times I(6 \times 6) \end{cases} \tag{45}$$

The expression of *RMSE* on the estimate is given by the following equation: $RMSE = \sqrt{(1/N)e^T e}$.

The expression of *RMSE* on the estimation of the position of the mobile robot is given by the following equation: $RMSE_r = \sqrt{RMSE_x^2 + RMSE_y^2}$.

The implementation results under Matlab are shown in Fig. 12 for the two algorithms. In order to evaluate the estimation accuracy, we calculated the *RMSE* on the estimate. Tab. 4 shows the results obtained.

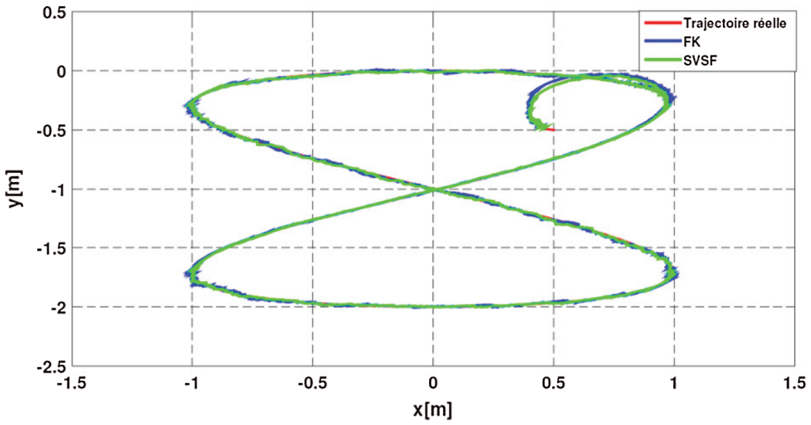

Figure 12: The trajectories estimated by the different algorithms

Table 4: Comparison of the different estimation algorithms with RMSE for Scenario 3

Scenario 3	KF	SVSF
RMSE on x	0.0133	0.0495
RMSE on y	0.0154	0.0284
RMSE (position)	0.0204	0.0571

It was found that the values of *RMSE* of the Kalman filter are lower than those of the SVSF. In this scenario we deduced that the estimation of the trajectory of the UGV by the KF is more accurate in comparison with the SVSF.

Scenario 4: In this scenario, unfavorable conditions for the Kalman filter will be considered, in order to show the efficiency, robustness and superiority of the SVSF with respect to the KF, when the initial conditions are poorly chosen (the initial conditions are increased by a factor of 10), so that noises on states and measurements are Gaussian, correlated, non-centered:

$$\begin{cases} Q_k = \Gamma \begin{bmatrix} 0.02^2 & 0.01^2 \\ 0.01^2 & 0.02^2 \end{bmatrix} \Gamma^T; \quad E[v_k] = \begin{bmatrix} 10^{-2} \\ 10^{-2} \end{bmatrix} \\ R_k = \begin{bmatrix} 0.05^2 & 0.02^2 \\ 0.02^2 & 0.05^2 \end{bmatrix}; \quad E[w_k] = \begin{bmatrix} 0.04 \\ 0.04 \end{bmatrix} \end{cases} \tag{46}$$

Fig. 13 shows the estimated trajectories of the UGV and the *RMSE* are given in Tab. 5.

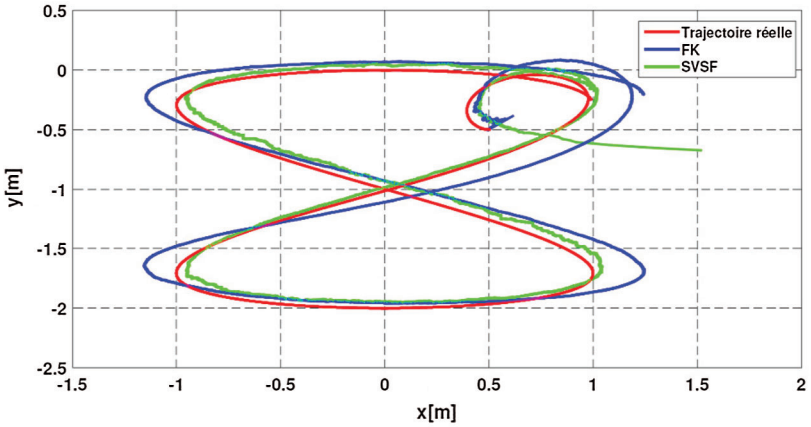

Figure 13: The estimated trajectories by different algorithms

Table 5: Comparison of the different estimation algorithms with RMSE for Scenario 4

Scenario 4	KF	SVSF
RMSE on x	0.0650	0.0548
RMSE on y	0.1500	0.0719
RMSE (position)	0.1635	0.0905

It was found that the values of $RMSE_x$, $RMSE_y$ and $RMSE_r$ are lower compared to those of KF which has poor estimation accuracy, due to the nature of the non-centered correlated noises and the poor choice of the initial conditions. Ultimately, the SVSF has also proven to be more robust, stable and accurate.

5.2 Robust Ground Agent Tracking using SVSF and IBC of UAV

In order to evaluate the performance of this architecture, we mainly integrate in this case two scenarios 1 and 2 described above and based on the results of estimation of the SVSF to carry out missions of tracking a ground agent. The initial conditions and constraints are the same. The initial parameters of the SVSF estimator are given in Eqs. (44) and (45).

From the results of Fig. 14, it is clear that the IBC control is more efficient. This control (Fig. 15) reduces tracking errors. For example, in Scenario 1, we obtained 0.08 m in x, y and 0.25 m in z (Fig. 16) with the BC 0.18 m errors in x, y and 0.35 m in z. Fig. 17 shows that the integral backstepping control has greatly reduced the effect of parametric uncertainties and measurement noises (scenario 2).

Thus, it can be deduced that the IBC makes it possible to obtain a better robustness with respect to the parametric uncertainties and a better rejection of the external disturbances with respect to the BC.

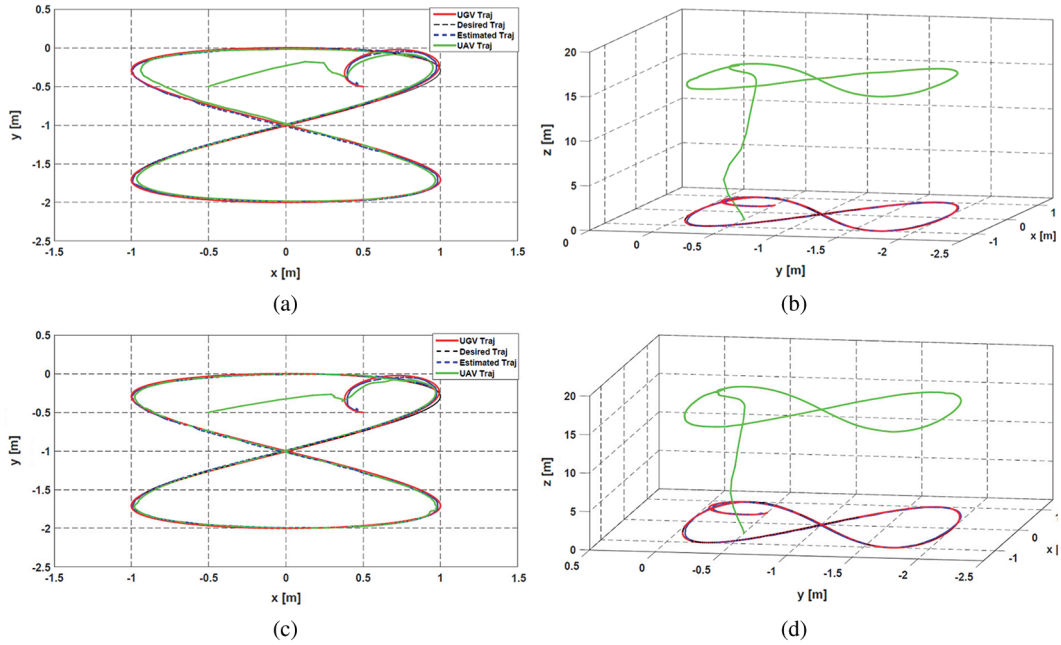

Figure 14: Tracking of UGV by UAV using SVSF and the IBC: scenario 1 ((a) 2D, (b) 3D), scenario 2 ((c) 2D, (d) 3D)

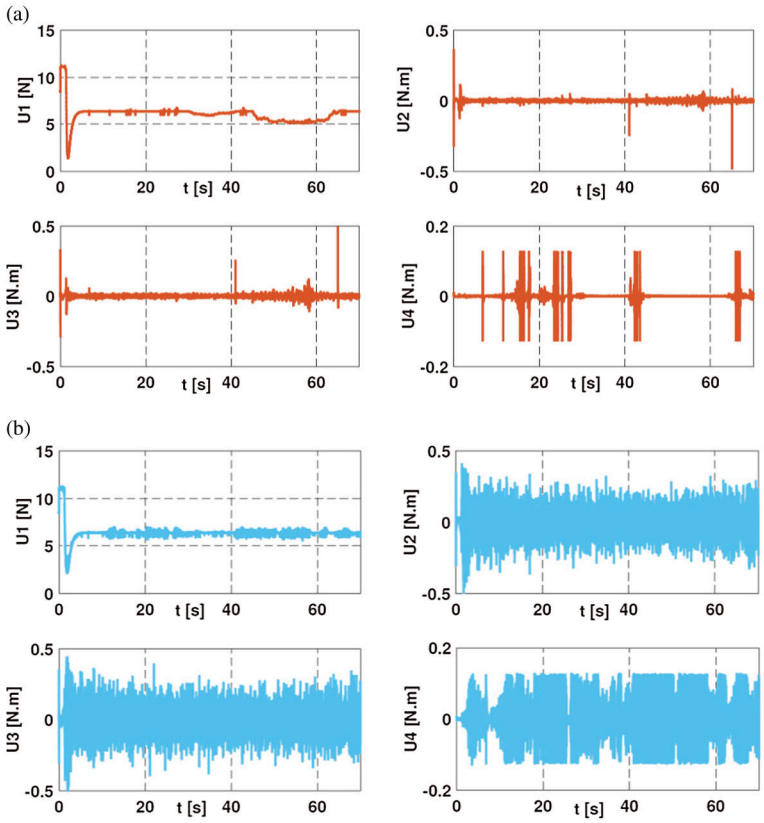

Figure 15: Integral backstepping control inputs of the quadrotor for different scenarios: (a) scenario 1, (b) scenario 2

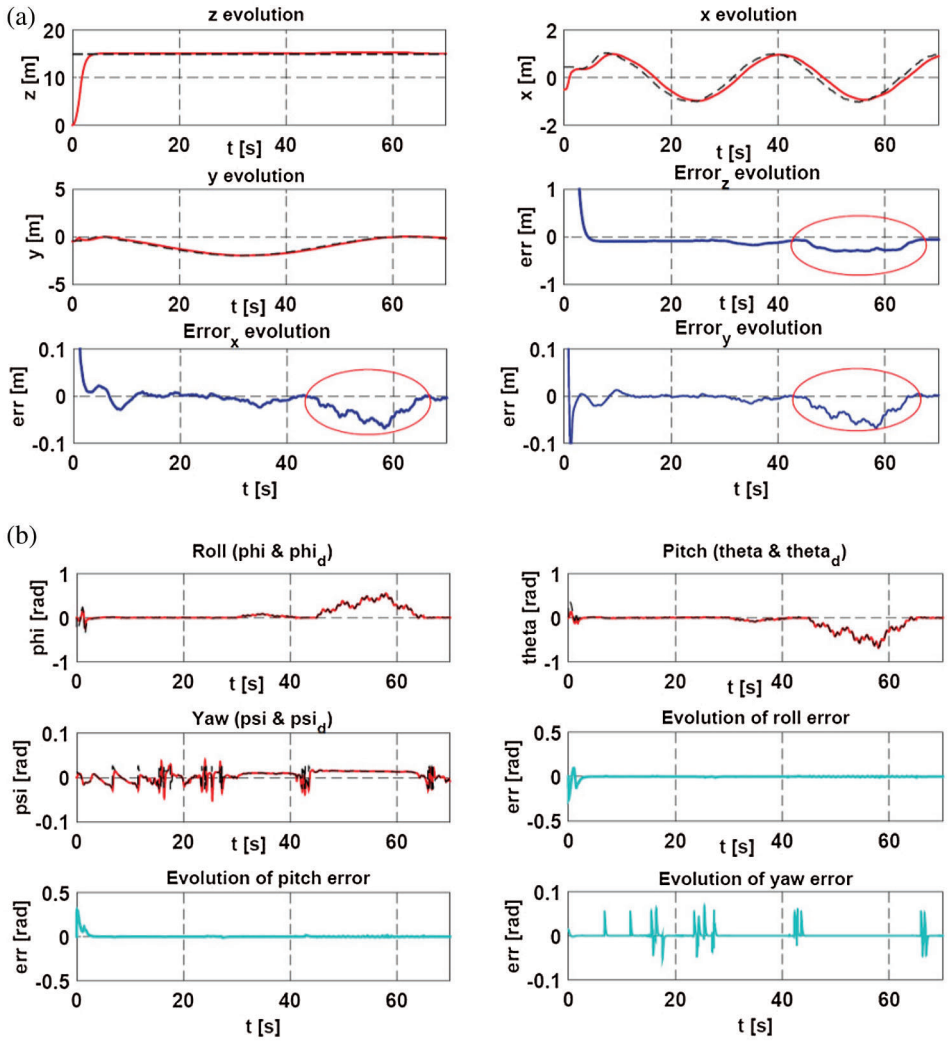

Figure 16: Evolution of the translation (x, y, z) and the angles of orientation of the quadrotor with wind disturbance respectively (a) and (b)

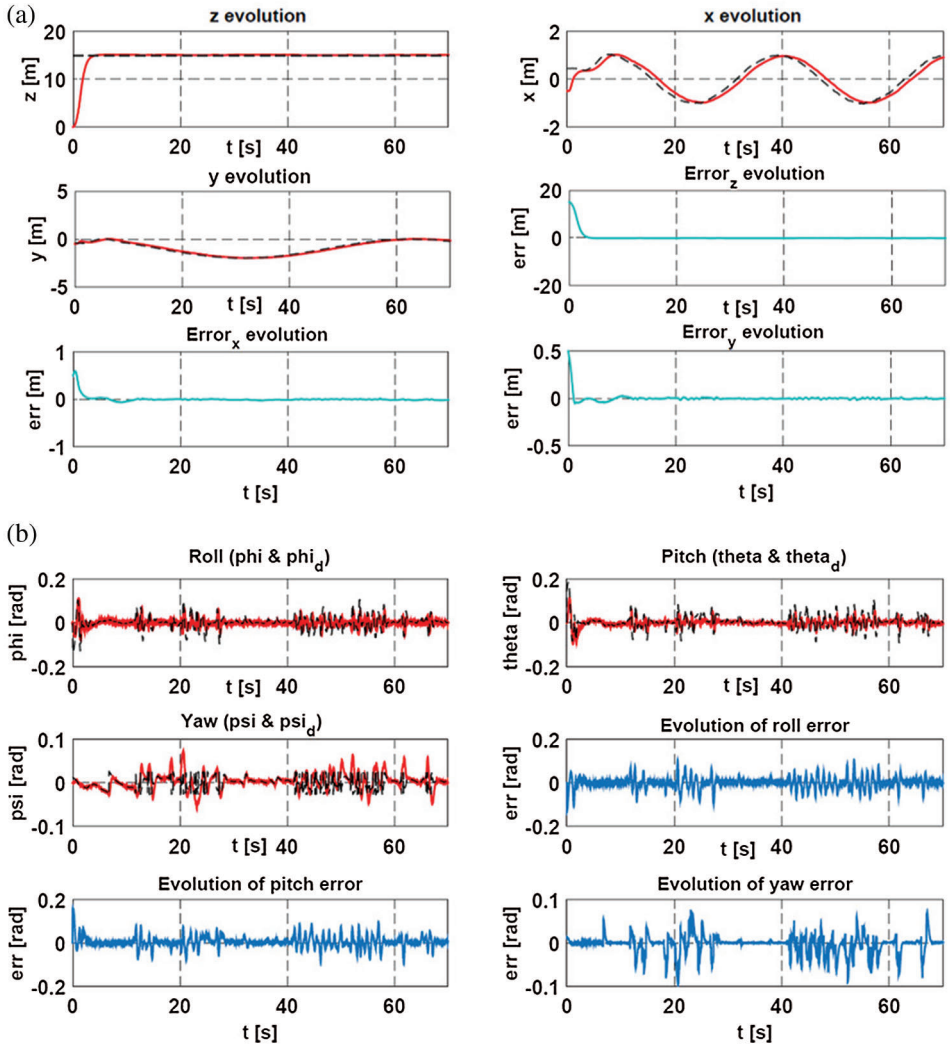

Figure 17: Evolution of the translation (x, y, z) and the angles of orientation of the quadrotor with parametric uncertainties and measurement noises respectively (a) and (b)

6 Conclusions

This paper proposed a robust control and tracking architecture in order to allow for an UAV to track an UGV in disturbed environment. The considered UGV is a Unicycle mobile robot. On one hand, the latter has been controlled based on the Integral Sliding Mode technique taking into account the kinematics constraints on the speed limitations. A tracking algorithm based on the Kalman filter was introduced in order to estimate the relative state of the UGV in a disturbed environment. On the other hand, a considered UAV type quadrotor and a backstepping controller is designed to stabilize this UAV. A first set of simulations was performed by considering several scenarios. The simulation results of this tracking architecture have shown limited robustness with respect to external disturbances, modeling errors and measurement noises.

In order to improve the performance of this architecture, the Kalman filter has been replaced by the Smooth Variable Structure Filter and the integral-backstepping controller was introduced in order to overcome the challenges of classical backstepping robustness. The stability of the synthesized control laws has been proved by the Lyapunov theory; which is necessary to achieve UGV/UAV cooperation

architecture. The second set of simulations considering the proposed architecture has shown the improvement of robustness and accuracy of this architecture.

Current and future works concern the implementation of the proposed architecture and algorithms on a Pixhawk autopilot for UAV control and Raspberry Pi based vision module for automated UGV target visual detection, recognition and tracking.

Acknowledgement: We would like to thank the staff of the Ecole Militaire Polytechnique of Algiers, especially Doctor Oualid Araar, for the assistance afforded to perform this research.

Funding Statement: The authors received no specific funding for this study.

Conflicts of Interest: The authors declare that they have no conflicts of interest to report regarding this study.

References

[1] E. H. C. Harik, F. Guinand, H. Pelvillain, F. Guérin and J. F. Brethé, "A decentralized interactive architecture for aerial and ground mobile robots cooperation," in *Proc. Int. Conf. on Control, Automation and Robotics*, Singapore, pp. 37–43, 2015.

[2] A. Ferrag, A. Oussar and M. Guiatni, "Robust coordinated motion planning for UGV/UAV agents in disturbed environment," in *Proc. 8th International Conference on Modelling, Identification and Control (ICMIC)*, Algiers, pp. 472–477, 2016.

[3] J. E. Gomez-Balderas, P. Castillo, J. A. Guerrero and R. Lozano, "Vision based tracking for a quadrotor using vanishing points," *Journal of Intelligent & Robotic Systems*, vol. 65, no. 1–4, pp. 361–371, 2012.

[4] C. C. Ke, J. G. Herrero and J. Llinas, "Comparison of techniques for ground target tracking," in *State University of New York At Buffalo Center Of Multisource Information Fusion, Rep. ADA400079*, 2000.

[5] F. Rafi, S. Khan, K. Shafiq and M. Shah, "Autonomous target following by unmanned aerial vehicles," *Unmanned Systems Technology VIII*, vol. 6230, pp. 10–18, 2006.

[6] R. Wise and R. Rysdyk, "UAV coordination for autonomous target tracking," in *Proc. AIAA Guidance, Navigation, and Control Conf. and Exhibit*, Colorado, pp. 6453–6475, 2006.

[7] C. Peterson and D. A. Paley, "Multivehicle coordination in an estimated time-varying flowfield," *Journal of Guidance, Control, and Dynamics*, vol. 34, no. 1, pp. 177–191, 2011.

[8] T. H. Summers, M. R. Akella and M. J. Mears, "Coordinated standoff tracking of moving targets: Control laws and information architectures," *Journal of Guidance, Control, and Dynamics*, vol. 32, no. 1, pp. 56–69, 2009.

[9] S. Kim, H. Oh and A. Tsourdos, "Nonlinear model predictive coordinated standoff tracking of a moving ground vehicle," *Journal of Guidance, Control, and Dynamics*, vol. 36, no. 2, pp. 557–566, 2013.

[10] S. A. P. Quintero, D. A. Copp and J. P. Hespanha, "Robust UAV coordination for target tracking using output-feedback model predictive control with moving horizon estimation," in *Proc. American Control Conf. (ACC)*, Chicago, pp. 3758–3764, 2015.

[11] J. Lee, R. Huang, A. Vaughn, X. Xiao and J. K. Hedrick, "Strategies of path-planning for a UAV to track a ground vehicle," in *AINS Conf.*, Sengupta, 2003.

[12] Y. Bar-Shalom, *Tracking and data association*. San Diego: Academic Press Professional, Inc., 1987.

[13] B. K. Ghosh and E. P. Loucks, "A realization theory for perspective systems with applications to parameter estimation problems in machine vision," *IEEE Transactions on Automatic Control*, vol. 41, no. 12, pp. 1706–1722, 1996.

[14] Y. Bar-Shalom, P. K. Willett and X. Tian, *Tracking and data fusion*. Storrs: YBS publishing, 2011.

[15] F. Capezio, A. Sgorbissa and R. Zaccaria, "GPS-based localization for a surveillance UGV in outdoor areas," in *Proc. the Fifth Int. Workshop on Robot Motion and Control (RoMoCo'05)*, Dymaczewo, pp. 157–162, 2005.

[16] C. C. Haddal and J. Gertler, *Homeland security: Unmanned aerial vehicles and border surveillance*. Library of Congress Washington DC Congressional Research Service, Rep. ADA524297, 2010.

[17] C. Pippin, G. Gray, M. Matthews, D. Price, A. P. Hu *et al.,* "The design of an air-ground research platform for cooperative surveillance," Georgia Tech Research Institute. Tech. Rep. 112010, 2010.

[18] A. M. Khaleghi, D. Xu, Z. Wang, M. Li, A. Lobos *et al.,* "A DDDAMS-based planning and control framework for surveillance and crowd control via UAVs and UGVs," *Expert Systems with Applications*, vol. 40, no. 18, pp. 7168–7183, 2013.

[19] M. Saska, T. Krajnik and L. Pfeucil, "Cooperative μUAV-UGV autonomous indoor surveillance," in *Proc. 9th Int. Multi-Conf. on Systems, Signals and Devices (SSD)*, Chemnitz, pp. 1–6, 2012.

[20] H. G. Tanner and D. K. Christodoulakis, "Cooperation between Aerial and Ground vehicle groups for Reconnaissance missions," in *Proc. of the 45th IEEE Conf. on Decision and Control*, San Diego, CA, pp. 5918–5923, 2006.

[21] B. Grocholsky, J. Keller and V. Kumar, "Cooperative air and ground surveillance," *IEEE Robotics & Automation Magazine*, vol. 13, no. 3, pp. 16–25, 2006.

[22] D. K. MacArthur and C. D. Crane, "Unmanned ground vehicle state estimation using an unmanned air vehicle," in *Proc. Int. Sym. on Computational Intelligence in Robotics and Automation*, Jacksonville, FI, pp. 473–478, 2007.

[23] S. Kanchanavally, R. Ordonez and J. Layne, "Mobile target tracking by networked uninhabited autonomous vehicles via hospitability maps," in *Proc. of the American Control Conf.*, Boston, MA, USA, pp. 5570–5575, 2004.

[24] R. Madhavan, T. Hong and E. Messina, "Temporal range registration for unmanned ground and aerial vehicles," *Journal of Intelligent and Robotic Systems*, vol. 44, no. 1, pp. 47–69, 2005.

[25] U. Zengin and A. Dogan, "Real-time target tracking for autonomous UAVs in adversarial environments: A gradient search algorithm," *IEEE Transactions on Robotics*, vol. 23, no. 2, pp. 294–307, 2007.

[26] J. Y. Choi and S. G. Kim, "Collaborative tracking control of UAV-UGV," *International Journal of Mechanical, Aerospace, Industrial, Mechatronic and Manufacturing Engineering*, vol. 6, no. 11, pp. 2487–2493, 2012.

[27] S. Ulun and M. Unel, "Coordinated motion of UGVs and a UAV," in *Proc. IECON 39th Annual Conf. of the IEEE Industrial Electronics Society*, Vienna, pp. 4079–4084, 2013.

[28] M. Saska, V. Vonásek, T. Krajník and L. Přeučil, "Coordination and navigation of heterogeneous UAVs-UGVs teams localized by a hawk-eye approach," in *Proc. IEEE/RSJ Int. Conf. on Intelligent Robots and Systems*, Vilamoura, pp. 2166–2171, 2012.

[29] L. Barnes, R. Garcia, M. Fields and K. Valavanis, "Swarm formation control utilizing ground and aerial unmanned systems," in *Proc. IEEE/RSJ Int. Conf. on Intelligent Robots and Systems*, Nice, pp. 4205–4205, 2008.

[30] N. Rackliffe, H. A. Yanco and J. Casper, "Using geographic information systems (GIS) for UAV landings and UGV navigation," in *Proc. IEEE Conf. on Technologies for Practical Robot Applications*, Woburn, MA, pp. 145–150, 2011.

[31] C. Phan and H. H. T. Liu, "A cooperative UAV/UGV platform for wildfire detection and fighting," in *Proc. Asia Simulation Conf.—7th Int. Conf. on System Simulation and Scientific Computing*, Beijing, pp. 494–498, 2008.

[32] P. Tokekar, J. V. Hook and D. Mulla, "Sensor planning for a symbiotic UAV and UGV system for precision agriculture," *IEEE Transactions on Robotics*, vol. 32, no. 6, pp. 1498–1511, 2016.

[33] D. Yulong, X. Bin, C. Jie, F. Hao and Z. Yangguang, "Path planning of messenger UAV in air-ground coordination," *IFAC-PapersOnLine*, vol. 50, no. 1, pp. 8045–8051, 2017.

[34] H. Abaunza, E. Ibarra, P. Castillo and A. Victorino, "Quaternion based control for circular UAV trajectory tracking, following a ground vehicle: Real-time validation," *IFAC-PapersOnLine*, vol. 50, no. 1, pp. 11453–11458, 2017.

[35] D. C. Guastella, L. Cantelli, C. D. Melita and G. Muscato, "A global path planning strategy for a UGV from aerial elevation maps for disaster response," in *Proc. 9th Int. Conf. on Agents and Artificial Intelligence(ICAART)*, Porto, pp. 335–342, 2017.

[36] J. Peterson, H. Chaudhry, K. Abdelatty and J. Bird, "Online aerial terrain mapping for ground robot navigation," Sensors, vol. 18, no. 2, pp. 630–652, 2018.

[37] S. Govindaraj, K. Chintamani and J. Gancet, "The ICARUS project—Command, control and intelligence (C2I)," in *Proc. IEEE Int. Sym. on Safety, Security, and Rescue Robotics (SSRR)*, Linkoping, pp. 1–4, 2013.

[38] S. Batzdorfer, M. Bobbe, M. Becker, H. Harms and U. Bestmann, "Multisensor equipped UAV/UGV for automated exploration," *The International Archives of Photogrammetry, Remote Sensing and Spatial Information Sciences*, vol. 42, pp. 33–41, 2017.

[39] M. Defoort, J. Palos, A. Kokosy, T. Floquet, W. Perruquetti *et al.,* "Experimental motion planning and control for an autonomous nonholonomic mobile robot," in *Proc. IEEE Int. Conf. on Robotics and Automation*, Roma, pp. 2221–2226, 2007.

[40] M. Asif, A. Y. Memon and M. J. Khan, "Output feedback control for trajectory tracking of wheeled mobile robot," *Intelligent Automation & Soft Computing*, vol. 22, no. 1, pp. 75–87, 2015.

[41] J. A. Ruz-Hernandez, E. N. Sanchez and M. Saad, "Real-time decentralized neural control for a five Dof redundant robot," *Intelligent Automation & Soft Computing*, vol. 19, no. 1, pp. 23–37, 2013.

[42] L. E. Zárate and P. Resende, "Fuzzy sliding mode controller for a PH process in stirred tanks," *Intelligent Automation & Soft Computing*, vol. 18, no. 4, pp. 349–367, 2012.

[43] M. H. Casado and F. J. Velasco, "Thruster control based on the shunt DC motors for a precise positioning of the marine vehicles," *Intelligent Automation & Soft Computing*, vol. 15, no. 3, pp. 425–438, 2009.

[44] S. Bogosyan, "A sliding mode based neural network for data fusion and estimation using multiple sensors," *Intelligent Automation & Soft Computing*, vol. 17, no. 4, pp. 477–493, 2011.

[45] Z. P. Jiang, E. Lefeber and H. Nijmeijer, "Saturated stabilization and tracking of a nonholonomic mobile robot," *Systems & Control Letters*, vol. 42, no. 5, pp. 327–332, 2001.

[46] M. Defoort, T. Floquet and A. Kokosy, "Integral sliding mode control for trajectory tracking of a unicycle type mobile robot," Integrated Computer-Aided Engineering, vol. 13, no. 3, pp. 277–288, Jul. 2006.

[47] R. Abbas and Q. Wu, "Formation tracking for multiple quadrotor based on sliding mode and fixed communication topology," in *Proc. 5th Int. Conf. on Intelligent Human-Machine Systems and Cybernetics*, Hangzhou, pp. 233–238, 2013.

[48] M. P. Aghababa and M. E. Akbari, "A chattering-free robust adaptive sliding mode controller for synchronization of two different chaotic systems with unknown uncertainties and external disturbances," *Applied Mathematics and Computation*, vol. 218, no. 9, pp. 5757–5768, 2012.

[49] X. R. Li and V. P. Jilkov, "Survey of maneuvering target tracking: Dynamic models," *Signal and Data Processing of Small Targets*, vol. 4048, pp. 212–236, 2000.

[50] S. Bouabdallah, "Design and control of quadrotors with application to autonomous flying," Ph.D dissertation. École Polytechnique Fédérale de Lausanne (EPFL), Lausanne, 2007.

[51] R. Mahony, V. Kumar and P. Corke, "Multirotor aerial vehicles: Modeling, estimation, and control of quadrotor," *IEEE Robotics & Automation Magazine*, vol. 19, no. 3, pp. 20–32, 2012.

[52] H. Khebbache, B. Sait, Naâmane Bounar *et al.,* "Robust stabilization of a quadrotor UAV in presence of actuator and sensor faults," *International Journal of Instrumentation and Control Systems*, vol. 2, no. 2, pp. 53–67, 2012.

[53] F. Yacef, O. Bouhali, M. Hamerlain and N. Rizoug, "Observer-based adaptive fuzzy backstepping tracking control of quadrotor unmanned aerial vehicle powered by Li-ion battery," *Journal of Intelligent & Robotic Systems*, vol. 84, no. 1–4, pp. 179–197, 2016.

[54] E. C. Suiçmez, "Trajectory tracking of a quadrotor unmanned aerial vehicle (UAV) via attitude and position control," Ph.D. dissertation. Middle East Technical University, Ankara, 2014.

[55] W. Gawronski, "Three models of wind-gust disturbances for the analysis of antenna pointing accuracy," Jet Propulsion Laboratory, California Institute of Technology, vol. 42, no. 149, IPN progress report, 2002.

[56] J. Wang, M. Geamanu, A. Cela, H. Mounier and S. Niculescu, "Event driven model free control of quadrotor," in *Proc. IEEE Int. Conf. on Control Applications (CCA)*, Hyderabad, pp. 722–727, 2013.

[57] T. Bandyopadhyay, N. Rong, M. Ang, D. Hsu and W. S. Lee, "Motion planning for people tracking in uncertain and dynamic environments," in *Proc. Workshop on People Detection and Tracking, IEEE Int. Conf. on Robotics and Automation*, Kobe, pp. 1935–1943, 2009.

[58] S. J. Godsill, J. Vermaak, W. Ng and J. F. Li, "Models and algorithms for tracking of maneuvering objects using variable rate particle filters," *Proceedings of the IEEE*, vol. 95, no. 5, pp. 925–952, 2007.

[59] A. Gadsden and S. Habibi, "Target tracking using the smooth variable structure filter," in *Proc. ASME Dynamic Systems and Control Conf.*, Hollywood, pp. 187–193, 2009.

[60] S. A. Gadsden, "Smooth variable structure filtering: Theory and applications," Ph.D. dissertation. McMaster University, Hamilton, 2011.

[61] S. Habibi, "The smooth variable structure filter," *Proceedings of the IEEE*, vol. 95, no. 5, pp. 1026–1059, 2007.

[62] S. R. Habibi and R. Burton, "The variable structure filter," in *Proc. ASME Int. Mechanical Engineering Congress and Exposition*, New Orleans, pp. 157–165, 2002.

[63] M. Al-Shabi, A. Saleem and T. A. Tutunji, "Smooth variable structure filter for pneumatic system identification," in *Proc. IEEE Jordan Conf. on Applied Electrical Engineering and Computing Technologies (AEECT)*, Amman, pp. 1–6, 2011.

[64] S. R. Habibi and R. Burton, "Parameter identification for a high-performance hydrostatic actuation system using the variable structure filter concept," *Journal of Dynamic Systems, Measurement, and Control*, vol. 129, no. 2, pp. 229–235, 2007.

[65] M. Attari, "SVSF estimation for target tracking with measurement origin uncertainty," Ph.D. dissertation. McMaster University, Hamilton, 2016.

[66] S. A. Gadsden and S. R. Habibi, "A new form of the smooth variable structure filter with a covariance derivation," in *Proc. 49th IEEE Conf. on Decision and Control (CDC)*, Atlanta, GA, pp. 7389–7394, 2010.

[67] M. Bouchoucha, S. Seghour, H. Osmani and M. Bouri, "Integral backstepping for attitude tracking of a quadrotor system," *Elektronika ir Elektrotechnika*, vol. 116, no. 10, pp. 75–80, 2011.

[68] M. Tahar, K. M. Zemalache and A. Omari, "Control of an under-actuated X4-flyer using integral backstepping controller," *Przegląd Elektrotechniczny*, vol. 87, no. 10, pp. 251–256, 2011.

[69] R. Rashad, A. Aboudonia and A. El-Badawy, "Backstepping trajectory tracking control of a quadrotor with disturbance rejection," in *Proc. XXV Int. Conf. on Information, Communication and Automation Technologies (ICAT)*, Sarajevo, pp. 1–7, 2015.

[70] F. Yacef, O. Bouhali, M. Hamerlain and A. Rezoug, "PSO optimization of integral backstepping controller for quadrotor attitude stabilization," in *Proc. 3rd Int. Conf. on Systems and Control*, Algiers, pp. 462–466, 2013.